Surface Chemistry and Electrochemistry of Supported Zerovalent Iron Nanoparticles in the Remediation of Aqueous Metal Contaminants

Sherman M. Ponder,[†] John G. Darab,[‡] Jerome Bucher,[§] Dana Caulder,[§] Ian Craig,[§] Linda Davis,[§] Norman Edelstein,[§] Wayne Lukens,[§] Heino Nitsche,[§] Linfeng Rao,[§] David K. Shuh,[§] and Thomas E. Mallouk*[,†]

Department of Chemistry, The Pennsylvania State University, University Park, Pennsylvania 16802, Pacific Northwest National Laboratory, Richland, Washington 99352, and Lawrence Berkeley National Laboratory, Berkeley, California 94720

Received April 6, 2000. Revised Manuscript Received November 17, 2000

The microstructure, physical characteristics, corrosion behavior, and reactivity of zerovalent iron nanoparticles synthesized on a support (primarily a nonporous, hydrophobic polymer resin) were studied. The remediation of groundwater by zerovalent iron in in situ permeable reactive barriers relies on the redox reaction between metallic iron and a reducible contaminant. Decreasing the size of the iron particles and dispersing them on a support increases the specific surface area of the iron, as well as the ratio of surface to bulk iron atoms, and should thereby increase both the reaction rate and the fraction of iron atoms available for the reaction. Borohydride reduction of aqueous ferrous sulfate gives supported iron nanoparticles, 10−30 nm in diameter, which consist of 85% zerovalent iron by weight. These materials ("ferragels") are stable in air and have corrosion behavior comparable to iron filings. Interestingly, the presence or absence of a support, as well as the boron remaining from the borohydride reduction process, influences the electrochemical corrosion rate of the composite materials. Supported and unsupported zerovalent iron nanoparticles are superior to iron filings in both terms of initial rates of reduction and total moles of contaminants (Cr(VI), Pb(II), TcO_4^-) reduced per mole of iron. The enhanced reactivity and passive corrosion behavior of these materials should make them good candidates for use in permeable reactive barriers.

Introduction

Permeable reactive barriers of zerovalent iron are an emerging technology for the remediation of contaminated groundwater streams.[1−3] In situ barriers have the advantage of providing a passive, continuous treatment of the groundwater plume, without requiring the ongoing maintenance and costs of a pump-and-treat physical plant.[4,5]

The reactive material used for these permeable barriers is usually zerovalent iron particles in the form of iron filings, which are inexpensive and readily available. Zerovalent iron is a strong reducing agent that reacts with water-borne chlorinated organics, nitroaromatics, radionuclides, and heavy metals.[6−14] Full reduction of the organics produces environmentally innocuous compounds, while reduction of the radionuclides and heavy metals renders them insoluble and immobile.

The standard half-cell reactions involving zerovalent iron and its reaction products are as follows:

$$Fe^{3+} + 3e^- \rightarrow Fe^0 \quad E_0 = -0.037\ V \qquad (1)$$

$$Fe^{2+} + 2e^- \rightarrow Fe^0 \quad E_0 = -0.447\ V \qquad (2)$$

and

* Corresponding author. Telephone: (814)863-9637. Fax: (814)863-8403. E-mail: tom@chem.psu.edu.
† The Pennsylvania State University.
‡ Pacific Northwest National Laboratory.
§ Lawrence Berkeley National Laboratory.

(1) Sweeney, K. H. (Envirogenics Systems Company, El Monte, CA) U.S. Patent 4,382,865, May 10, 1993.
(2) Gillham, R. W. (University of Waterloo) U.S. Patent 5,534,154, July 9, 1996.
(3) Sivavec, T. M.; Horney, D. P.; Bahel, S. S. (General Electric Company, Schnectady, NY) U.S. Patent 5,575,927, November 19, 1996.
(4) Powell, R. M.; Puls, R. W.; Blowes, D. W.; Vogan, J. L.; Gillham, R. W.; Powell, P. D.; Schultz, D.; Landis, R.; Sivavec, T. *Permeable Reactive Barrier Technologies for Contaminant Remediation.* U. S. Environmental Protection Agency, 1998; EPA/600/R-98/12.
(5) Beitinger, E. *Permeable Treatment Walls-Design, Construction, and Cost*, Special Session on Treatment Walls and Permeable React; U. S. Environmental Protection Agency: Vienna, Austria, 1998; EPA 542-R-98-00, 6−16.
(6) Gillham, R. W.; O'Hannesin, S. F. *Ground Water* **1994**, *32*, 958.
(7) Matheson, L. J.; Tratnyek, P. G. *Environ. Sci. Technol.* **1994**, *28*, 2045.
(8) Orth, W. S.; Gillham, R. W. *Environ. Sci. Technol.* **1996**, *30*, 66.
(9) Burris, D. R.; Campbell, T. J.; Manoranjan, V. S. *Environ. Sci. Technol.* **1995**, *29*, 2850.
(10) Powell, R. M.; Puls, R. W.; Hightower, S. K.; Sabatini, D. A. *Environ. Sci. Technol.* **1995**, *29*, 1913.
(11) Boronina, T.; Klabunde, K. J.; Sergeev, G. *Environ. Sci. Technol.* **1995**, *29*, 1511.
(12) Blowes, D. W.; Ptacek, C. J.; Benner, S. G.; McRae, C. W. T.; Puls, R. W. *Groundwater Quality: Remediation and Protection, IAHS Pub. no. 250*, **1998**, 483.
(13) Smith, E. H. *Water Res.* **1996**, *30*, 2424.

10.1021/cm000288r CCC: $20.00
Published on Web 01/04/2001

$$Fe^{3+} + e^- \rightarrow Fe^{2+} \quad E_0 = +0.771\ V \qquad (3)$$

Since eqs 1 and 2 are heterogeneous reactions, and since the oxidation of Fe^{2+} also involves solid products at neutral or basic pH, the surface area of the solid iron has a direct influence on the number of active surface sites presented to the groundwater plume.[15] Decreasing the iron particle size should increase the surface area and thereby the rate of reaction. Increasing the specific surface area should also result in an increase in the fraction of iron atoms that are on the particle surface, thereby creating a greater reductive capacity per gram. This may allow the use of smaller amounts of iron to treat the contaminated plume. The ability to reduce excavation size through the use of thinner barriers and smaller excavations is an important consideration, because excavation is the largest capital cost in the use of in situ permeable barriers.[5]

We have recently reported that resin-supported zerovalent iron ("ferragel") is far superior to iron filings in the batch remediation of Cr(VI) and Pb(II).[16] Chromium is reduced to the 3+ oxidation state, apparently in the form of a chromite, consistent with the findings of other groups,[17,18] and lead is reduced to Pb(0). In both cases, iron is oxidized to 3+ and forms an insoluble oxide. Initial reduction rates are 3−5 times higher for iron-on-resin ferragel than they are for an equivalent weight of iron filings. The rates depend on both the amount of iron added to the solution as well as the initial concentration of contaminant, and show mixed zero- and first-order kinetics.[19,20]

Per mole of iron, ferragels reduced 20−30 times more contaminant (initial concentration 0.50 mM) than did commercial iron filings. Batch tests run for 60 days showed that 90% of the reduction occurred within the first 48 h of exposure regardless of whether the iron was in the form of supported or unsupported nanoparticles, or iron filings. All of these results suggest that supported iron nanoparticles are an interesting candidate for use in permeable reactive barriers.

The stability of zerovalent iron is an important consideration in reactive barrier applications. This is because iron reacts not only with the contaminants in the plume, which are generally present at low concentrations, but also with dissolved oxygen and with water itself:

$$2Fe^0_{(s)} + O_{2(g)} + 4H^+ \rightarrow 2Fe^{2+}_{(aq)} + 2H_2O_{(l)} \qquad (4)$$

$$Fe^0_{(s)} + 2H_2O \rightarrow Fe^{2+}_{(aq)} + H_{2(g)} + 2OH^-_{(aq)} \qquad (5)$$

Groundwater plumes are relatively anoxic in comparison to surface streams. However, freshwater, as well as the dissolved oxygen it carries, is constantly supplied by the groundwater flow in an immobile, underground barrier. Since it can require 100−200 years for a contaminant plume to flow past a physical point, the corrosion behavior of the barrier components is of high importance.

Corrosion may be quantified by using a version of the Butler−Volmer equation[21] to follow the current−voltage behavior under kinetically limited conditions:

$$i = i_{corr}(e^{-\beta_c(E-E_{corr})} - e^{\beta_a(E-E_{corr})}) \qquad (6)$$

Here, i is the net current density, i_{corr} is corrosion current density, E is the potential, and E_{corr} is the corrosion potential. β_c and β_a are the slopes in the cathodic and anodic Tafel regions of plots of ln $|i|$ versus potential.[22] E_{corr} is the potential at which the system is in equilibrium and no current flows. Thus i_{corr} may be found at the intersection of the extrapolated linear regions of the Tafel curves, and in a simple system this intersection occurs at E_{corr}. Since current density is directly proportional to the standard rate constant, k^0, the relative magnitude of i_{corr} gives a measure of reaction kinetics, and may be converted to engineering terms using the following equation:

$$R = (MW/n\rho F)(i_{corr}) \qquad (7)$$

where R is the corrosion rate in meter per second, MW is the molecular weight (0.05585 kg/mol for iron), n is the number of electrons exchanged (2 e^-), ρ is the density of the metal (7870 kg/m^3), and F is the Faraday constant.[23] Multiplication by 3.2×10^{10} converts the corrosion rate into mm/year.

Tafel behavior is observed at both negative and positive overpotentials under irreversible conditions, i.e., far from equilibrium, before mass transfer becomes limiting. In these potential regions, one of the exponential terms in eq 6 becomes much smaller than the other—effectively reducing it to zero—and a linear relation between ln $|i|$ and E appears. The slopes of the curves in these two regions are

$$\beta_a = \frac{(1-\alpha)nF}{2.3RT} \text{ for the anodic branch} \qquad (8)$$

and

$$\beta_c = \frac{(\alpha)nF}{2.3RT} \text{ for the cathodic branch} \qquad (9)$$

where α is the barrier asymmetry factor, n is the number of electrons, F is the Faraday constant, R is the gas constant, and T is the absolute temperature. The slope of lower magnitude of these two equations indicates the half-reaction for which the rate varies more slowly with E. Thus, an anodic slope that is smaller than the cathodic slope implies that the rate of reaction is

(14) Farrell, J.; Bostick, W. D.; Jarabek, R. J.; Fiedor, J. N. *Ground Water* **1999**, *37*, 618.
(15) Wang, C.-B.; Zhang, W.-X. *Environ. Sci. Technol.* **1997**, *31*, 2154.
(16) (a) Ponder, S. M.; Darab, J. G.; Mallouk, T. E. *Environ. Sci. Technol.*, in press. (b) Ponder, S. M.; Ford, J. R.; Darab, J. G.; Mallouk, T. E. *Mater. Res. Soc. Symp. Proc.* **1999**, *556* (Scientific Basis for Nuclear Waste Management XXII), 1269−1276.
(17) Pratt, A. R.; Blowes, D. W.; Ptacek, C. J. *Environ. Sci. Technol.* **1997** *31*, 2492.
(18) Blowes, D. W.; Ptacek, C. J.; Jambor, J. L. *Environ. Sci. Technol.* **1997**, *31*, 3348.
(19) Wust, W. F.; Kober, R.; Schlicker, O.; Dahmke, A. *Environ. Sci. Technol.* **1999**, *33*, 4304.
(20) Gotpagar, J. K.; Grulke, E. A.; Bhattacharyya, D. *J. Haz. Mater.* **1998**, *62*, 243.
(21) Bard, A. J.; Faulkner, L. R. *Electrochemical Methods;* J. Wiley & Sons: New York, 1980; pp 86−114.
(22) Farrell, J.; Kason, M.; Melitas, N.; Li, T. *Environ. Sci. Technol.* **2000**, *34*, 514.
(23) West, J. M. *Basic Corrosion and Oxidation*, 2nd ed.; J. Wiley & Sons: New York, 1986; pp 85−94.

limited by the anodic process, i.e., oxidation of iron, rather than by cathodic processes such as reduction of oxygen, water, or contaminants.[22]

Passivation of the surface of a metal such as iron occurs when surface sites become saturated with a metal oxide, or other species, which lowers the exchange current density, and thereby drastically reduces k^0. Under these conditions, the transfer of electrons from zerovalent iron becomes the limiting step in the reaction, and k^0 becomes small. The lower valent oxides of iron, wustite ($Fe_{1-x}O$) and magnetite (Fe_3O_4), are much better electronic conductors than goethite (α-FeOOH).[24] Precipitated goethite therefore forms a passivating layer—the most passivating of any of the commonly oxidized iron species.

In this study, we examine the surface chemistry and corrosion of supported iron nanoparticles and compare them with other forms of zerovalent iron. These nanoparticles are made by borohydride reduction of an aqueous iron salt in the presence of the support. The support itself is intended to disperse the iron particles, thereby increasing the total specific surface area (m^2/g iron exposed at the surface), and to provide for greater hydraulic conductivity by preventing agglomeration of the iron nanoparticles.

Experimental Section

Ferragel Synthesis and Batch Testing. The syntheses of ferragel and unsupported nano-iron, as well as the experimental procedure for batch tests of ferragel and Cr or Pb solutions, have been previously described.[16] The same procedures were followed here with the exception that the pH was adjusted by adding 10.00 mL of 0.100 M Na_2CO_3, instead of 3.8 M NaOH, in the synthesis of the resin-supported ferragel. In the preparation of the latter, PolyFlo (Puresyn, Malvern PA), a hydrophobic resin, was used. In addition, a poorly crystalline zirconium oxide powder obtained from Pacific Northwest National Laboratory (20−40 μm) and silica gel (200−400 mesh, Aldrich) were also used as support materials. Iron filings (~40 mesh, Fisher), iron powder (−325 mesh [<45 μm], J. T. Baker), and electrolytically pure iron chunks (10−30 mesh, 99.999%, Aldrich) were all used as obtained.

Corrosion Testing. Corrosion studies on the powders were performed using a recently developed "sticky carbon" rotating disk electrode (RDE) method.[25] An RDE with the disk removed (Pine Instruments), leaving a 2 mm-deep well, was filled with a warmed 65% beeswax (Aldrich)/35% acetylene carbon black (Aldrich) (w/w) mixture. The mixture in the well was compressed by hand, allowed to cool, and then polished using the surface of ordinary weighing paper. Powder impression was performed by weighing a single layer of the powder onto the outlined area of a glass microscope cover slide marked with the circumference of the beeswax/carbon well, warming the electrode end slightly until the carbon surface began to lose its glossiness, and then manually impressing the end of the electrode into the powder. The balance used was a Mettler Toledo AB204 (±0.0002 g).

The electrode tip was submerged in a three-neck flask containing 65 mL of 0.1 M $KClO_4$ aqueous solution and rotated at 2500 rpm for 12−16 hours to allow for equilibration. The lengthy equilibration times appeared necessary to stabilize the rest potentials. Linear voltammetry was performed without removing the electrode from the flask, at a rotation rate of 2500 rpm, from −1500 to +1500 mV at a scan rate of 1 mV/s using an EG&G model 363 potentiostat/galvanostat. A platinum wire or mesh served as the counter electrode, and Ag/AgCl was the reference electrode. All voltages are reported versus SHE. The sample size was 0.9−1.4 mg of powder for ferragel or nano-iron samples and 10−12 mg for iron filings. Reproducibility for the corrosion experiments was within 1.0 $\mu A/cm^2$.

Analytical Measurements. Iron contents were determined using acid dissolution followed by atomic absorption spectroscopy (AAS) on a Perkin-Elmer 530 atomic adsorption spectrometer. X-ray powder diffraction (XRD) was performed using a Phillips X'Pert MPD diffractometer. X-ray photoelectron spectroscopy (XPS) was performed on a Kratos XSAM800 pci. Nitrogen BET surface analysis was performed using a Micromeritics ASAP 2010. Thermal gravimetric analysis (TGA) was performed on a TGA2050 thermogravimetric analyzer (TA Instruments), in air, with a temperature ramp of 10 °C/min. Scanning electron microscopy (SEM) was performed on a JEOL JSM 5400 microscope, whereas transmission electron microscopy (TEM) was performed on a JEOL 1200EXII microscope. Densities were determined by water displacement.

Initial X-ray absorption near-edge structure (XANES) spectra were obtained at room temperature on beam line X19A at the National Synchrotron Light Source (NSLS). The data were obtained in transmission mode using samples prepared by thinly distributing powdered samples (−325 mesh) of iron-on-poorly crystalline ZrO_2 ferragel, as well as hematite (α-Fe_2O_3), on cellophane tape. The beam line used a Si (111) double-crystal monochromator and standard ionization detectors. For each scan, the incident and transmitted X-ray intensities were recorded as a function of X-ray energy. Data for the near edge spectrum were collected starting at 7012 eV. (The Fe K edge is 7112 eV for Fe metal). Monochromator step increments were 0.5 eV between 7072 and 7262 eV. X-ray energies were calibrated using an iron metal foil as a reference. Between three and five scans were taken for each sample, depending on the strength of the signal, and averaged. Each set of averaged XANES data was then normalized with respect to its step height.

Results and Discussion

Materials Characterization. *Iron Content and Particle Size.* The iron-on-resin ferragels used in this study contained 22.6% iron by weight, as determined by AAS. The surface area of the material was 24.4 ± 1.5 m^2/g, with little or no hysteresis in nitrogen BET analysis. The surface area, by nitrogen BET, of the nonporous resin itself, after treatment with borohydride (but in the absence of iron) was 3−3.5 m^2/g, depending on the average diameter of the particles. The surface area of unsupported nano-iron, synthesized in the absence of a support material, was 21.7 ± 1.5 m^2/g. The density of resin-supported ferragel was 1.1 g/cm^3. Densities of 6.7 and 6.8 g/cm^3, respectively, were found for the iron filings and iron powder, as received. The lower densities of the commercial iron materials (compared to pure iron, 7.87 g/cm^3) were not unexpected. AAS analysis of these materials showed a bulk iron content of about 80%. XPS indicated that the surface of the iron filings contained approximately 60 atom % carbon.

As a comparison, a ferragel was made using porous silica gel particles as support. The density of silica-supported ferragel was 1.3 g/cm^3. The iron content of silica gel-supported ferragels was equivalent to that of resin-supported ferragels, but the surface area was 239 ± 2 m^2/g, compared to an initial surface area of about 440 m^2/g for the silica itself. The surface area of the silica-supported material was comparable to that of metallized aerogels recently described, although the method of preparation was different.[26]

(24) Cornell, R. M.; Schwertmann, U. *The Iron Oxides*; VCH Publishers: New York, 1996; p 100.

(25) Long, J. W.; Rolison, D. R. *Proc.—Electrochem. Soc.* **1999** (New Directions in Electroanalytical Chemistry II), pp 125−131.

Iron grain sizes were calculated from BET data, assuming spherical nanoparticles and were also determined by measurement of TEM micrographs. The techniques agreed reasonably to give an average iron particle diameter of 10−30 nm.

The borohydride reduction of iron sulfate yielded nanoparticles of zerovalent iron that were similar in terms of size and surface area regardless of whether a support material was used. It was immediately apparent in the synthesis that pH had a strong effect on iron particle size in the reaction product. Filtration times for ferragel employing the same amounts of reagents and time of reaction may range from 5 to 10 min for materials prepared at pH 5, to more than 5 h for materials prepared in basic solution. The ferragels described in this study were prepared by adjusting to slightly acidic pH (6.2−6.8) prior to borohydride addition. The pH was adjusted by adding either NaOH or Na_2CO_3 to the aqueous mixture. No attempt was made to control the pH during the reduction reaction; no additional buffering agents were added.

The surface areas of the unsupported nano-iron and the resin support were approximately additive to give the surface area of resin-supported ferragel. In contrast, the reduced surface area of silica gel-supported ferragel suggested that not only do the silica pores contain zerovalent iron, but that a significant portion of the iron is occluded in these pores and blocked from surface interactions. Although the silica-supported ferragel had an order of magnitude higher specific surface area, the resin-supported ferragel was faster in remediating Cr(VI) and Pb(II) solutions in batch tests.[16]

SEM images of the silica-supported ferragel showed evidence of aggregation and dendritic crystal growth of the iron. In contrast, the iron-on-resin ferragel was relatively featureless. Higher magnification TEM images showed small aggregates of iron nanoparticles widely dispersed across the resin surface. (See Figure 1.) XANES of freshly prepared ferragel showed that about 15% of the total iron was present as Fe(III), while 85% was zerovalent iron. (See Figure 2) No evidence of Fe(II) was found in the solid. The presence of oxidized iron was not surprising since zerovalent iron ignites in air, yet ferragels are stable in air (at least up to one year) once dried. Thus, much, if not all, of the oxidized iron forms a protective oxide layer preventing this combustion. XPS of freshly prepared zirconia-supported ferragel showed all of the surface iron in the 3+ oxidation state, which implies complete oxidation at least to the XPS sampling depth of ca. 25 Å.

Some care was required during the synthesis of ferragel to prevent oxidation of zerovalent iron. During filtration of the solid, the iron nanoparticles were very susceptible to oxidation due to the presence of oxygen, water, and salts formed in the reduction process. Powder XRD showed that the most prevalent crystalline end-product of this oxidation was goethite, α-FeOOH. However, the small size of the iron particles limited the detectability of minor iron oxide components, and thus, other iron oxide or oxyhydroxide species may also have been present. The use of the ethanol washes during filtration avoided most of this oxidation. Without the ethanol washes, nearly all of the iron was visibly oxidized before the filtration was complete.

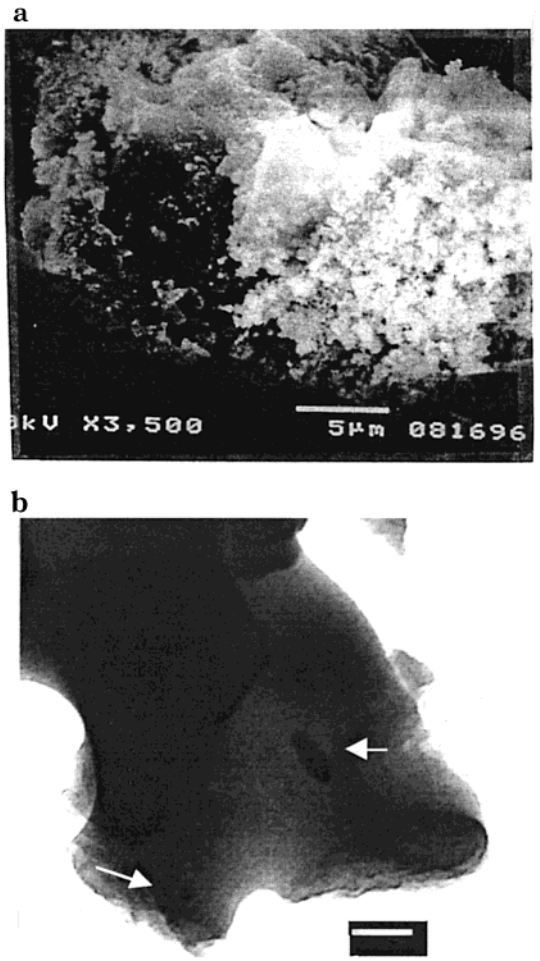

Figure 1. Top: SEM image of a single particle of iron-on-silica gel ferragel showing bright, electrically charged, dendritic crystallites of iron on the particle surface. Scale bar is 5 μm. Bottom: TEM image of iron-on-resin ferragel showing widely dispersed crystallites of iron (highlighted by arrows) on the resin surface. Scale bar is 50 nm.

Surface Water and Hydration. TGA analysis of unsupported nano-iron showed a maximum weight loss of 7% at 255 °C, a third of which occurred below 100 °C. The water loss in this region is consistent with the physisorption of 1.4 mol of water/mol of oxidized (surface-exposed) Fe, assuming that the surface contains 15% of the iron as Fe^{3+} (See Figure 3). Weight loss at higher temperatures show that an average of 2.7 mol of water are bound per mole of iron atoms on the surface to form a hydrated (oxy)hydroxide or oxide. The weight gain between 255° and 560° was consistent with a gain of 1.2 mol of oxygen/mol of zerovalent iron. Since the observed weight gain does not take into account additional loss of water or hydrogen above 255°, this calculation underestimates the oxygen uptake and is therefore not inconsistent with the formation of hematite (α-Fe_2O_3). Heating unsupported nano-iron at 600° for 2 h produced hematite, as determined by XRD.

In contrast, the maximum water loss for iron filings was 0.14% (6 mmol H_2O/mole Fe) at 386 °C. The total weight gain was 0.155% between 386 and 629 °C. These results suggest that most of the accessible iron on the filings was already oxidized. They also suggest that

(26) Anderson, M. L.; Morris, C. A.; Stroud, R. M.; Merzbache, C. I.; Rolison, D. R. *Langmuir* **1999**, *15*, 674.

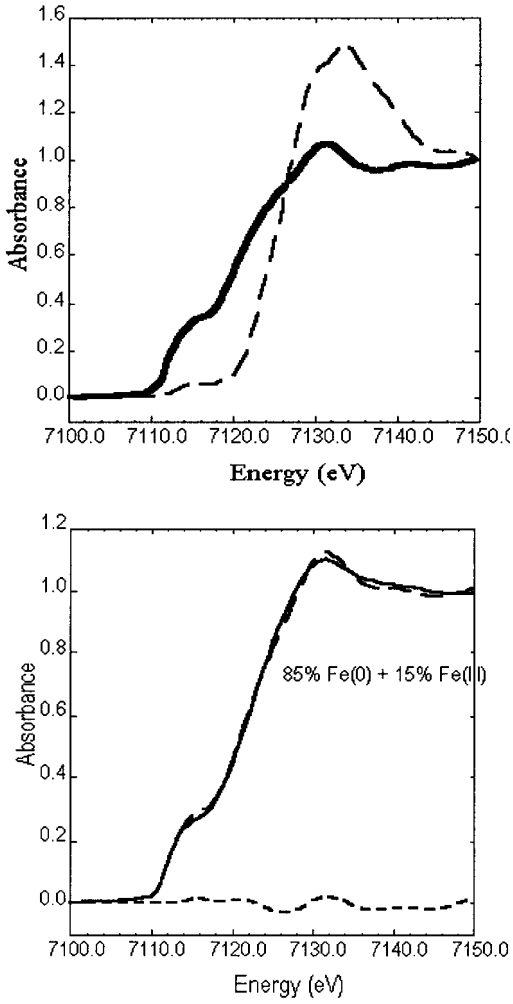

Figure 2. Top: XANES spectra of iron foil and hematite standards. Bottom: XANES spectra of iron-on-zirconia ferragel showing the fit to 85% Fe^0 and 15% Fe(III), and the difference between the fit and the spectra. In this particular case, analysis was performed on a zirconia-supported ferragel. The zirconia support is strongly resistant to highly alkaline solutions such as that found in U.S. DOE military tank wastes stored at Hanford, WA.

there may be a limit to the "shelf life" of ferragels. The iron nanoparticles contain considerably more water, both physisorbed and chemisorbed, than do the larger particles in iron filings. While ferragels do not lose their reducing power over the period of a year or more, longer term exposure to air may ultimately dehydrate them to form less porous and less reactive surface oxides.

Boron Content. While it is a physically simple process, the borohydride reduction of aqueous metal salts is a complex reaction that is sensitive to a surprising number of parameters. Besides the effect of pH on iron particle size, it has previously been reported that the concentration of the borohydride solution and its rate of addition alter the composition of the reaction product.[27] The reaction of Fe^{2+} with $NaBH_4$, in the absence of a support, yields a product which contains 10−12 atom % boron in the bulk (by ICP-AES), and 22.5 atom % B on the surface (by XPS). Approximately 90% of the surface boron has a binding energy of 192 eV, consistent

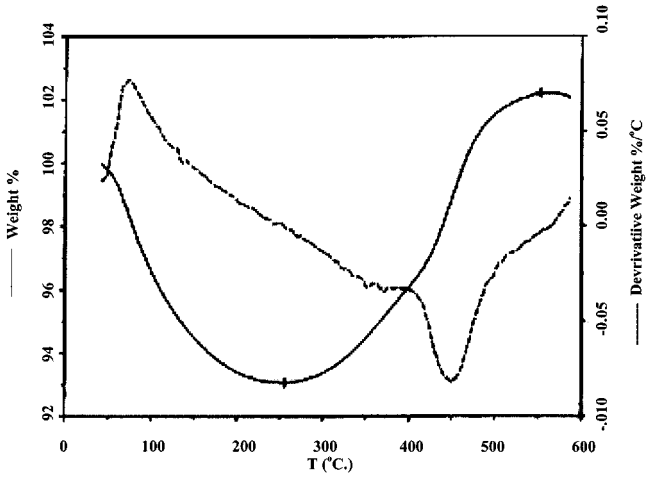

Figure 3. TGA of unsupported nano-iron showing water loss peak at 255 °C and oxidation peak at 560 °C. Dashed line is the first derivative of the curve and shows more clearly the range of temperatures for the vaporization of physisorbed water on the left, and the combustion/oxidation to hematite on the right.

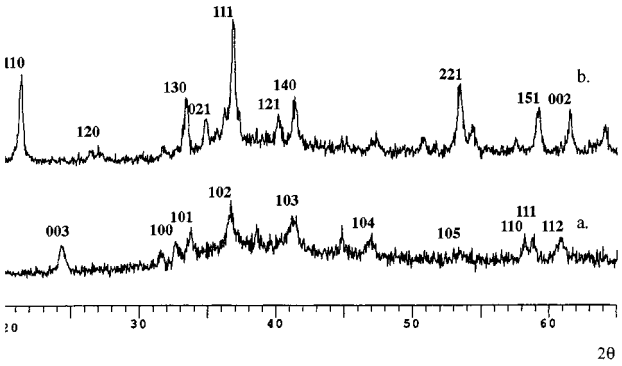

Figure 4. XRD patterns of resin-supported ferragel. **(**a**)** Diffraction pattern of damp ferragel showing the Miller indices of green rust (hexagonal $Fe_2O_3 \cdot xH_2O$). (b**)** The same ferragel after 2 weeks exposure to atmosphere showing the Miller indices of orthorhombic goethite (α-FeOOH).

with the 3+ oxidation state. The remainder has a binding energy of 188 eV, consistent with the zerovalent state. Thus, the surface of the iron nanoparticles is relatively enriched in boron, which is present on the surface as a salt, and little, if any, iron boride is present in the bulk. This is in contrast to the metal borides found as a major reaction product of the borohydride reduction of aqueous salts of other transition metals.[27−30]

Corrosion in an Aqueous Environment. While a fully vacuum-dried ferragel contains mostly zerovalent iron, XRD of a resin-supported ferragel that was removed from vacuum while still damp showed an initial powder pattern consistent with the formation of green rust, $Fe_2O_3 \cdot xH_2O$.[24] (See Figure 4.). Although the material was made from ferrous sulfate, it is not clear that sulfate was the supporting anion in this green rust. After 2 weeks of further aging of this damp ferragel, XRD showed the formation of goethite. The fact that these XRD patterns show an endproduct of goethite, with intermediate green rust, indicates that the environment,

(27) Shen, J.; Li, Z.; Yan, Q.; Chen, Y. *J. Phys. Chem.* **1993**, *97*, 8504.

(28) van Wonterghem, J.; Morup, S.; Koch, C. J. W.; Charles, S. W.; Wells, S. *Nature* **1986**, *322*, 622.

(29) Kiessling, R. *Acta Chem. Scand.* **1950**, *4*, 209.

(30) Shen, J.; Hu, Z.; Hsia, Y.; Chen, Y. *Appl. Phys. Lett.* **1991**, *59*, 2510.

at least at the iron surface, is a reducing environment with pH around 5−7. In contrast, an oxidizing environment with pH ≥8 typically produces maghemite.[31−33]

Corrosion tests of the various iron-bearing powders on a "sticky carbon" electrode failed to provide a definitive rate of corrosion for the iron particles. (See Figure 5.) Instead, the experiments demonstrated that both the support material and the preparation method have a strong effect on the bulk electrochemical reaction of the composite materials.

Figure 5a presents the corrosion of commercial iron filings, unsupported nano-iron, iron-on-silica gel ferragel, and iron-on-resin ferragel. All four curves show passivation of the iron and passive corrosion that is strongly anodically controlled. E_{corr} for all forms of iron tested is about −25 mV. The corrosion current density measured from these plots, i_{corr}, is 6.3×10^{-5} A/m^2 for both the iron filings and the unsupported nano-iron, 7.9×10^{-6} A/m^2 for the iron-on-resin, and 2.0×10^{-6} A/m^2 for the iron-on-silica. These i_{corr} figures would seem to indicate that the iron passively corrodes much more slowly on the composite materials. In parts a and c of Figure 5, the same data are plotted as log |current/g Fe| versus millivolts (SHE) and log |current| versus millivolts (SHE), respectively. Normalizing the curves to the mass of iron in the composite seems to indicate that the lower current per gram of Fe present in the filings could provide a much lower passive corrosion rate than those of any of the forms of nanoparticles. These results are in direct contrast to Figure 5a. However, it is clear from Figure 5c that the total current is comparable for all of the iron-bearing materials. Thus, the conclusion may be drawn from these three figures that the iron in these materials is not the controlling factor for passive oxidation in these experiments.

Parts a and b of Figure 6 demonstrate that the reaction products of the borohydride reduction process are the major component of the passive corrosion curves obtained in these experiments. The untreated support materials, as expected, show very low reactivity. However, the same support materials, when treated by the borohydride reduction process, but in the absence of any iron salt, show plots that are remarkably similar to those of the iron-bearing composites. Thus, the conclusion may be drawn from Figures 5 and 6 that the iron in these materials is not the controlling factor for the passive oxidation found by these experiments.

Figures 5 and 6 suggest that the boron, or other reduced species, formed during the borohydride reduction process plays a central role in the passive corrosion behavior of the composite material. The boron, possibly in the form of HBO_2 or H_3BO_3 or an amorphous mixture with the iron oxide on the surface of the material, also appears to affect initial passive corrosion activity. Lengthy equilibration times were required before the rest potential of the system stabilized in these experiments. The electrochemical half reaction for boron is

$$H_3BO_3 + 3H^+ + 3e^- \rightarrow B^0 + 3H_2O \quad E° = -0.87\ V \tag{10}$$

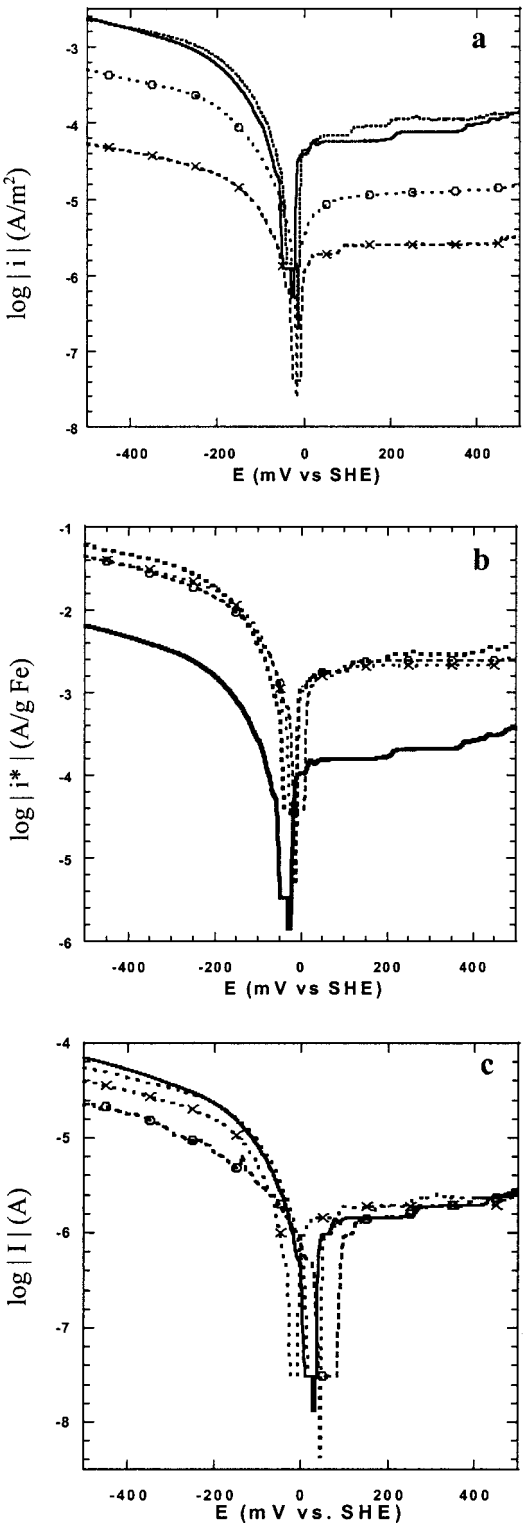

Figure 5. (a) log |current density (A/m^2)| vs potential (surface area is calculated for the composite material, including both the iron and the support), (b) log |current density/g Fe (A/g Fe)| vs potential, and (c) log |current (A)| vs potential: — = iron filings, – – – = unsupported nano-iron, -o- = resin-on-resin, -×- = silica-on-silica.

In summary, electrochemical corrosion testing of the composite powders did not provide a quantitative picture of the background corrosion rate of nanoscale iron.

(31) Schwertmann, U.; Cornell, R. M. *Iron Oxides in the Laboratory: Preparation and Characterization*; VCH Publishers: New Yotk, 1991; p 12.

(32) Nagayama, M.; Cohen, M. *J. Electrochem. Soc.* **1962**, *109*, 781.

(33) Bonin, P. M. L.; Odziemkowski, M. S.; Gillham, R. W. *Corros. Sci.* **1998**, *40*, 1391.

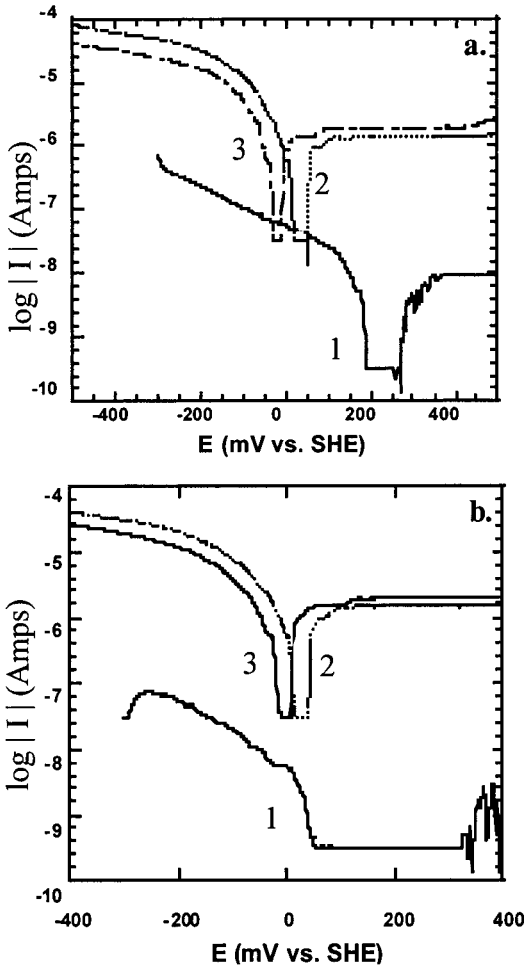

Figure 6. log |current (A)| versus potential. (a) 1 = untreated silica gel, 2 = silica gel treated with borohydride reduction in the absence of iron, and 3 = silica-on-silica gel. (b) 1 = untreated resin, 2 = resin treated with borohydride reduction in the absence of iron, and 3 = iron-on-resin.

In no case did the i_{corr} exceed that of iron filings, however. Thus, it may be concluded that nano-iron does not passively corrode more quickly than bulk forms of iron. However, whether the passive corrosion rate of supported nano-iron is much lower than that of bulk iron cannot be determined because of background activity of the support materials.

Most interestingly, the active corrosion of the composite materials—meaning the remediation of aqueous contaminant ions—is controlled by the nano-iron content. Borohydride-treated support materials that do not contain iron show minimal activity as remediants.[16] In contrast, passive corrosion—oxidation due to reaction with water and dissolved oxygen—appears to be controlled primarily by the products of the borohydride reduction process, and not by the iron.

Future Concerns for Applications. Supported and unsupported nano-iron are clearly superior to iron filings in short-term batch remediation reactions of aqueous Cr(VI), Pb(II), and TcO_4^-.[16] The initial rates of remediation, the total moles of contaminant reduced, and the lower initial corrosion rate all point to a significantly higher atom efficiency for iron nanoparticles. However, there are still some points that must be investigated before ferragels can be evaluated against more commonly used permeable barrier materials.

Table 1. Summary of Physical Characteristics of Various Types of Iron-Bearing Materials[a]

	ferragel (mL/g)	iron filings (mL/g)	ratio (ferragel/fil.)
dry, uncompressed	1.60	0.32	5.0
water displace., uncompressed	0.90	0.15	6.0
water displace., compressed to 1 ton pressure (600 psi)	.72	.15	4.8
water displace., compressed to 4.4 ton pressure (2900 psi)	.72	.17	4.2

[a] Comparison of volumes of ferragel and iron filings under various conditions. Compression was performed using an IR pellet press at 1.5×10^4 kPa. The resulting pellet was removed from the die for testing.

One concern is the corrosion behavior of ferragel over an extended time period. As noted, a groundwater plume may require 100−200 years to flow past a given point. Thus, the barrier material must react with a continuously replenished stream of low concentration of contaminant. None of the batch tests performed so far provide a constant supply of freshwater and dissolved oxygen as would be present in column or field applications. While tests indicate equivalent or better corrosion activity for resin-supported ferragel than for iron filings, accelerated corrosion tests under more realistic conditions are needed.

Another concern is the added volume necessary to include a support material in the bulk. Ferragels contain only about one-quarter the total iron per gram as iron filings, and the presence of the resin support increases the overall bulk by about a factor of 5. (See Table 1.) Since excavation is the highest capital cost for in situ barriers, the volume of the bulk material is an important consideration. Batch tests have shown that equivalent weights of resin-supported ferragel can reduce 21 times more Cr(VI) (0.50 mM) than iron filings on the basis of moles of iron present, and that this disparity widens as the contaminant concentration is lowered.[16] Thus, it is expected that ferragel can overcome the inherent disadvantage of increased volume while still outperforming iron filings. Again, this remains to be conclusively demonstrated with column and field tests.

Finally, hydraulic conductivity is a concern for barriers that are intended to be permeable. Groundwater flows are highly sensitive to changes in permeability, and an emplaced barrier is useless if the hydraulic conductivity of the barrier is sufficiently different from the surrounding environment as to redirect the flow of contaminant to the outside of the barrier. Since the relative volumes of compressed ferragel and iron filings remain nearly unchanged from the uncompressed volumes, it may be expected that ferragels will behave in a manner similar to iron filings. In field tests so far, alteration of hydraulic conductivity has not been an important parameter for iron filings barriers.

Ferragels may also offer the additional advantage of making deeper emplacements possible. By altering the size of the support, it may prove easier to use ferragels for direct injection into deeper-running groundwater flows.[34] There are also the possibilities of pelletization of ferragel,[35] or even, with the latitude provided by the

(34) Cantrell, K. J.; Kaplan, D. I. *J. Environ. Eng.* **1997**, *123*, 499.
(35) Li, Z.; Jones, H. K.; Bowman, R. S.; Helferich, R. *Environ. Sci. Technol.* **1999**, *33*, 4326.

high atom efficiencies, mixing sand or gravel into the barrier to improve hydraulic conductivity. None of these options have yet been explored and remain to be demonstrated with column and field tests.

Acknowledgment. This work was supported by the U.S. Department of Energy under Contract DE-FG07-97ER14822. Pacific Northwest National Laboratory is operated for the U.S. Department of Energy by the Battelle Memorial Institute under Contract DE-AC06-76RLO 1830. Electron microscopy and X-ray microanalysis were performed at the Electron Microscope Facility for the Life Sciences in the Biotechnology Institute at the Pennsylvania State University.

CM000288R